Wind and Structures, Vol. 13, No. 4 (2010) 347-362
DOI: http://dx.doi.org/10.12989/was.2010.13.4.347

Numerical simulation study of the Reynolds number effect on two bridge decks based on the deterministic vortex method

Zhiyong Zhou[1] and *Rujin Ma[2]

[1]*State Key Laboratory for Disaster Reduction in Civil Engineering, Tongji University, Shanghai, 200092, China*
[2]*Department of Bridge Engineering, Tongji University, Shanghai, 200092, China*
(Received August 22, 2008, Accepted February 22, 2010)

Abstract. Researches on the Reynolds number effect on bridge decks have made slow progress due to the complicated nature of the subject. Heretofore, few studies on this topic have been made. In this paper, aerostatic coefficients, Strouhal number (S_t), pressure distribution and Reynolds number (R_e) of Great Belt East Bridge and Sutong Bridge were investigated based on deterministic vortex method (DVM). In this method, Particle Strength Exchange (PSE) was chosen to implement the simulation of the flow around bluff body and to analyze the micro-mechanism of the aerostatic loading and Reynolds number effect. Compared with the results obtained from wind tunnel tests, reliability of numerical simulation can be proved. Numerical results also showed that the Reynolds number effect on aerostatic coefficients and Strouhal number of the two bridges can not be neglected. In the range of the Reynolds number from 10^5 to 10^6, it has great effect on the Strouhal number of Sutong Bridge, while the S_t is difficult to obtain from wind tunnel tests in this range.

Keywords: bridge sections, Reynolds number effect, particle strength exchange method, aerostatic coefficients, Strouhal number.

1. Introduction

As more streamlined decks and longer bridges are being built, the traditional practice of neglecting the Reynolds number effect on bridge decks produces more and more engineering problems. The Reynolds number effects on wind resistant design and analysis of large bridges are complex issues. In conventional wind resistant design of bridges, wind tunnel tests are highly relied upon, in which the similarity of the Reynolds number were often neglected. All parameters obtained from wind tunnel tests can be affected by the Reynolds number. According to the study proposed by Scanlan (Scanlan 1975), if the scale ratio is less than 1:300, more attention should be paid to the Reynolds number effect. However, the scale ratios of full bridge models were greater than this value even at that time. Before his death, he pointed out again that the Reynolds number effect should be adequately addressed.

* Corresponding Author, Lecturer, E-mail: rjma@tongji.edu.cn

Schewe is the first person who paid attention to the Reynolds number on bridge sections. In 1980s, Schewe (1983) made many researches of the Reynolds number effect on cylinder, as well as H-type sections and bridge decks in pressure wind tunnel. He found the existence of the Reynolds number effect on these kinds of sections. However, his research had attracted few attentions at that time. Recently, Schewe did many studies on the Reynolds number effect on the shape of wake flow around airfoil, cylinder and bridge deck (Great Belt East Bridge) (Schewe 2001). He found that the Reynolds number effect affected aerostatic coefficients by its influence on the shape of wake flow. Barré found the aerostatic coefficients of three section models of Normandy Bridge, whose scale ratios are 1:10, 1:50 and 1:20 respectively, did not coincide to each other, especially for the curves of lift coefficient vs. attack angle (Barré and Barnaud 1995). His conclusion was that those differences were due to the Reynolds number effect. When Great Belt East Bridge was under construction with 193 m deck completed, vortex excited vibration were observed. The difference between the shape of deck under construction and that of section model was firstly suspected. Afterwards, Larsen proved the existence of the Reynolds number effect in pressure wind tunnel tests (Schewe and Larsen 1998). Great difference of vortex excited vibration amplitude of section model tests with scale ratio of 1:20 and 1:80 was found in wind tunnel tests for Stonecutter Bridge in Hong Kong, which were thought as Reynolds number effect too.

Enlightened by Roshko, Larsen carried out flow visualization experiments under different Reynolds numbers (Schewe and Larsen 1998), when he was doing research on the Reynolds number effect of Great Belt East Bridge. The height of wake flow after flow separation at different Reynolds numbers was schematically plotted in Fig. 1. He found that, when the Reynolds number was less than 4×10^5, the separation point was located before the transition point. The separated flow will never re-attach, and the height of wake flow decreases with the increasing of the Reynolds number, as well as the drag force coefficient. When the Reynolds number is greater than 4×10^5, the separation point was located after the transition point. The separated flow will re-attach to the bottom of deck, but will never secondary re-attach. The height of wake flow varies a little with increasing of the Reynolds number, while the drag force coefficient decreases.

Experimental methods were found to be the best way to investigate the Reynolds number effect. Nowadays, numerical methods are being utilized to discover the micro mechanism of the Reynolds number effect. Vortex methods have been shown to be an attractive and successful approach for the numerical simulation of incompressible fluid flow at high Reynolds number (Leonard 1980, Sarpkaya 1989, Taylor and Vezza 1999, Walther and Larsen 1997, Zhou *et al*. 2003, Zhou and Chen 2006a, b). The basic idea of the vortex method for the simulation of viscous fluid flow is the fractional method (viscous splitting algorithms). In actual numerical calculation, the Euler equations are solved by using a vortex blob method and the viscous effect is simulated by a random walk or a deterministic method. In 1973, Chorin (1973) overcame the problem of the singularity of point vortex method by replacing the exact vorticity with the convolution of the vorticity with a cutoff

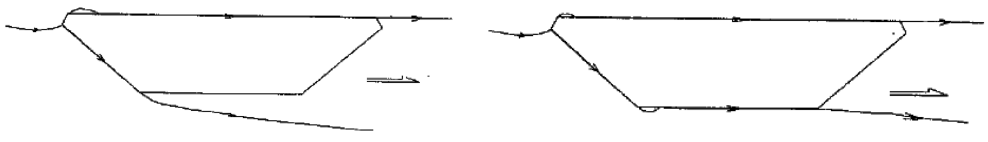

(a) Low Reynolds number (b) High Reynolds number

Fig. 1 Schematic diagram for the height of wake flow after flow separation vs. R_e

function, which approximates the delta function. Chorin also introduced the technique of random walk to simulate viscosity. The random walk method is popular and has been successfully applied to a number of situations. However, this method has large statistical errors occurred in the solution of vorticity and the rate of convergence for this method is low, although the statistical error for velocity is much smaller.

In recent years, several types of deterministic vortex methods have been proposed by Fishelov (1990), Cottet (1990), Shankar and Van Dommelen (1996). Cottet proposed an alternative approach of the core spreading algorithm, based on the analysis given by Degond and Mas-Gallic (1989): The weights of vortex particles are changed at each time step without changing their positions such that the conservation property of vorticity is satisfied. Unlike most vortex methods, Fishelov (1990) also proposed a deterministic method in which the diffusion of vorticity is also approximated by changing the particle weight rather than their positions and the vorticity field is approximated by using the second-order derivatives of the Laplacian operator by explicit differentiation of the cut-off function. In this way, Fishelov obtains much smaller numerical errors than for the random walk method.

Particle Strength Exchange (PSE) was developed from a different approach. Earlier work by Choquin and Huberson (1989) and Cottet and Mas-Gallic (Cottet 1990) involved a viscous splitting of the Navier-Stokes equations, with the diffusive component solved by means of a convolution with the heat kernel. Degond and Mas-Gallic (1989) developed the method in greater detail and presented a treatment for general convection–diffusion problems. They first approximate the Laplacian by an integral operator and then discretize the integral by a quadrature over the particles. Their techniques is now commonly known as PSE because of the conservation properties that are inherent when two particles “exchange strength” with one another. Particle strength exchange has been used extensively in vortex methods. The accuracy of the approach was explored by Choquin and Lucquin-Desreux (1988) on model problems and compared with that of the random walk method. Winckelmans and Leonard (1993) used the technique to account for viscous diffusion in three-dimensional simulations of vortex rings. Koumoutsakos *et al.* (1994) used it in conjunction with a wall flux treatment in their development of boundary conditions for viscous vortex methods. Ploumhans and Winckelmans (2000) adopted the method to account for particles of different core sizes and developed an image treatment near walls to remove spurious vorticity flux.

In this paper, deck sections of Great Belt East Bridge and Sutong Bridge, seen in Fig. 2, were investigated based on deterministic vortex method (DVM). The Reynolds number effect on aerostatic coefficients and Strouhal number was studied. In DVM, particle strength exchange method was chosen to treat viscosity diffusion. The reason for choosing these two bridge sections is that both of them have wind tunnel test data under different Reynolds number (Schewe and Larsen 1998, Chen 2004).

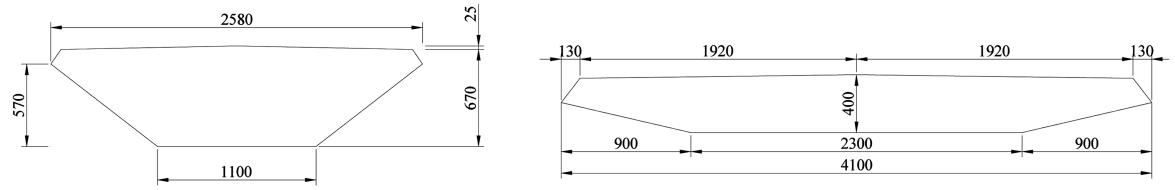

(a) Great Belt East Bridge (b) Sutong Bridge

Fig. 2 Two box girder sections discussed in this paper (unit: cm)

2. Mathematical format of particle strength redistribution method

2.1 Governing equations of vortex method and discretization of vorticity field

The kinematic relationship between the velocity field and the vorticity field is obtained by solving the following Poisson equation

$$\Delta u(x, t) = -\nabla \times \omega \tag{1}$$

When the flow around solid configuration in motion, Eq. (1) may be formulated as an integral equation, the generalized Biot-Savart integral

$$u(x, t) = U_{\infty}(t) - \frac{1}{2\pi}\iint_{f} \omega_f \times K(x_f - x)df + \frac{1}{2\pi}\int_{S} \frac{(u_s \cdot n_s)(x_s - x) - (u_s \times n_s) \times (x_s - x)}{|x_s - x|^2} dS \tag{2}$$

with,

$$K(x_f - x) = \frac{x_f - x}{|x_f - x|^2}$$

where $\boldsymbol{U}_{\infty}(t)$ is the free stream velocity, $\boldsymbol{n}_s$ is the outward normal vector of the solid boundary, f is the fluid region and S is the solid boundary and $\boldsymbol{u}_S(\boldsymbol{x}_S, t)$ is the solid velocity on the surface(S) at $\boldsymbol{x}_S$.

At the solid boundary, the fluid velocity $\boldsymbol{u}(\boldsymbol{x}_b, t)$ must be equal to the solid velocity ($\boldsymbol{u}(\boldsymbol{x}_S, t)$)

$$\boldsymbol{u}(\boldsymbol{x}_s, t) \cdot \boldsymbol{n}_S = \boldsymbol{u}_b(\boldsymbol{x}_b, t) \cdot \boldsymbol{n}_S; \quad \boldsymbol{u}(\boldsymbol{x}_s, t) \times \boldsymbol{n}_S = \boldsymbol{u}_b(\boldsymbol{x}_b, t) \times \boldsymbol{n}_S \ \ on\ S \tag{3}$$

With,

$$\boldsymbol{u}_s(\boldsymbol{x}_b, t) = \boldsymbol{u}_h(\boldsymbol{x}_b, t) + \Omega(t)\boldsymbol{e}_z \times (\boldsymbol{x}_c(t) - \boldsymbol{x}_b(t))$$

where $\boldsymbol{u}_h(\boldsymbol{x}_b, t)$ is the vertical velocity of the solid, Ω (t) is the rotational angular velocity and $\boldsymbol{x}_c$ is the center of mass.

At infinity we have

$$\boldsymbol{u}(\boldsymbol{x}, t) = \boldsymbol{U}_{\infty}(t) \quad when \quad x \to \infty \tag{4}$$

In the discrete vortex methods, the vorticity field is considered as a discrete sum of the individual vorticity fields of the particles, having core radius σ, strength Γ (t) and an individual distribution of vorticity determined by the function f_σ so that

$$\omega_f(\boldsymbol{x}, t) \doteq \omega_\sigma(\boldsymbol{x}, t) = \sum_{i=1}^{N_V} \Gamma_i(t) f_\sigma(\boldsymbol{x} - \boldsymbol{x}_i) \tag{5}$$

where N_V is total number of the vortex particle, which is described as vortex blob.

2.2 Applying non-slip boundary condition by viscosity splitting technique

Viscosity splitting technique is often used to solve convection and diffusion of vortices field of flow. In this technique, step-by-step algorithm is employed to solve the convection item and

viscosity item in Navier-Stokes equation. Correspondingly, applying non-slip boundary condition is based on viscosity splitting technique.

2.2.1 Solving region integral equation by panel method

The generalized Biot-Savart integral Eq. (2) is valid for both the fluid domain (f) and the solid domain (B). Owing to the generation of the fluid vorticity in the boundary region, we introduce a fluid layer, S^+ adjacent to the solid surface, S. When the thickness of the fluid layer f_s extend to infinitesimal, it is convenient to introduce the surface vortex sheet (SVS) γ_{s^+}. As a consequence, we have the following vector equation.

$$\boldsymbol{u}(\boldsymbol{x}, t) = \boldsymbol{U}_\infty(t) - \frac{1}{2\pi}\iint_f \omega_f \times K(x_f - x)df + \frac{1}{2\pi}\int_S \frac{(\boldsymbol{u}_s \cdot \boldsymbol{n}_s)(\boldsymbol{x}_s - \boldsymbol{x}) - (\boldsymbol{u}_s \times \boldsymbol{n}_s) \times (\boldsymbol{x}_s - \boldsymbol{x})}{|\boldsymbol{x}_s - \boldsymbol{x}|^2} dS \quad (6)$$

According to Eq. (6), we have the following vector equation for each vortex sheet γ_{s^+} in discrete form

$$\sum_{j=1}^{N_s} \int_{S_j} \frac{\gamma_{s^+} e_z \times (x_{S^+} - x_S)}{|\boldsymbol{x}_{S^+} - x_S|^2} dS = \sum_{j=1}^{N_s} \left\{ \int_{S_j} \frac{(u_S \cdot n_S)(x_S - x_{S^+}) - (u_S \times n_S) \times (x_S - x_{S^+})}{|\boldsymbol{x}_S - x_{S^+}|^2} dS \right\} + \int\int_{f-S^+} \omega_f \times K(x_f - x_{S^+})df + 2\pi[U_\infty(t) - u_S(x_{S^+})] \quad (7)$$

where $u_S(x_{S^+})$ is the velocity on the boundary of the solids at x_{S^+}. N_s is the number of the solids.

The normal and tangential components of the vector Eq. (7) are the first Fredholm integral equations in unknown γ_{s^+} and its solution is not unique according to the nature of Fredholm integral equation. The solution may be made unique by imposing a constraint based on the principle of the conservation of total vorticity. According to the principle, the total vorticity does not change with time.

$$\partial\left(\iint_f \omega df + \sum_j^{N_S} 2\Omega_j A_j \right) / \partial t = 0 \quad (8)$$

where Ω_j, Aj are the rotational angular velocity and the area of the j-th solid, respectively.

Using Eq. (5) in Eq. (8), in discrete form, the following equations can be obtained

$$\left\{ \sum_{i=1}^{N_v^k} \Gamma_i^k + \sum_{j=1}^{N_S} 2\Omega_j^k A_j + \sum_{j=1}^{N_S} \sum_{i=1}^{M_j} \gamma_{i,j}^k l_{i,j} \right\} - \left\{ \sum_{i=1}^{N_v^{k-1}} \Gamma_i^{k-1} + \sum_{j=1}^{N_S} 2\Omega_j^{k-1} A_j + \sum_{j=1}^{N_S} \sum_{i=1}^{M_j} \gamma_{i,j}^{k-1} l_{i,j} \right\} / \Delta t = 0 \Rightarrow$$
$$\sum_{j=1}^{N_S} \sum_{i=1}^{M_j} \gamma_{i,j}^k l_{i,j} = -\Gamma^{a,k-1} - 2\sum_{j=1}^{N_s} (\Omega_j^k - \Omega_j^{k-1}) A_j \quad \text{with} \quad \Gamma^{a,k-1} = \sum_{i=1}^{N_v^k} \Gamma_i^k - \left\{ \sum_{i=1}^{N_v^{k-1}} \Gamma_i^{k-1} + \sum_{j=1}^{N_S} \sum_{i=1}^{M_j} \gamma_{i,j}^{k-1} l_{i,j} \right\} \quad (9)$$

where N_v^k is the total number of vortex blob during the *k*-th time step, Γ_i^k is the circulation of *i*-th vortex blob at *k*-th time step, $l_{i,j}$ is the length of the i-th boundary element on the j-th solid surface, M_j is the total number of boundary elements on the *j*-th solid and $\Gamma^{a,k-1}$ is the total circulation of vortex blobs that have entered bodies and have been removed from numerical calculation during the

(k-1)-th time step.

The principle of the conservation of the total vorticity is applied to each body; as a consequence, the following equations can be obtained

$$\sum_{i=1}^{M_j} \gamma_{i,j}^{k} l_{i,j} = -\Gamma_j^{a,k-1} - 2(\Omega_j^k - \Omega_j^{k-1})A_j \qquad j = 1,2,\cdots,N_s \tag{10}$$

where $\Gamma_j^{a,k-1}$ is total circulation of the vortex blobs entered j-th solid during the (k-1)-th time step.

In this paper, the normal component of Eqs. (6), (9) and (10) are solved by applying the least square method.

2.2.2 High accuracy format for diffusion of boundary vortices

In this paper, vortex flux is applied to diffuse the boundary vortices to existed vortex blob, that is to say, non-slip boundary condition is satisfied by changing the strength of particle. When vortex sheet disappears from the surface of solids at the time of $[t,t+\delta t]$, the circulation (Γ) in the region of flow should be modified correspondingly.

$$\int \gamma(s)ds = \int_t^{t+\delta t} \frac{d\Gamma}{dt'} dt' \tag{11}$$

According the Kelvin rules, if the vortex flux is considered to be constant in a small time interval δt, the following equation can be obtained.

$$\nu \frac{\partial \omega}{\partial n}(s) = -\gamma(s)/\delta t \tag{12}$$

In this paper, the circulation of particles is determined by a high accuracy boundary vortices diffusion method.

$$\frac{d\Gamma_i}{dt} = \frac{\gamma}{\Delta t}\left([erfc(u)]_{\frac{x_i + h_i/2}{\sqrt{4\nu t}}}^{\frac{x_i - h_{i,l}/2}{\sqrt{4\nu t}}} \cdot \left(\sqrt{4\nu t}\frac{1}{2}\left([ierfc(s)]_{\frac{(y_i - b/2) + h_i/2}{\sqrt{4\nu t}}}^{\frac{(y_i - b/2) - h_i/2}{\sqrt{4\nu t}}} - [ierfc(s)]_{\frac{(y_i + b/2) + h_i/2}{\sqrt{4\nu t}}}^{\frac{(y_i + b/2) - h_i/2}{\sqrt{4\nu t}}} \right) \right) \right) \tag{13}$$

in which, $erfc(u) = \int_u^{\infty} \frac{2}{\sqrt{\pi}} \exp(-s^2) ds$, $ierfc(s) = \int_S^{\infty} erfc(v) dv = \frac{1}{\sqrt{\pi}} \exp(-s^2) - s erfc(s)$. When $0 < x_i < h_i$, $h_{i,l}/2 = x_i$. In other cases, $h_{i,l}/2 = h_i/2$. The first-layer particles can be made near or more greater than $h/2$, which guarantees the convergence of this method. The circulation can be obtained by integrating Eq. (13) in time history.

3. Solution to Navier-Stokes equation

Viscosity splitting technique is applied in solving Navier-Stokes equation. Viscosity splitting technique is a method, by which the convection item and viscosity item is solved step by step in one time step.

3.1 Calculation of convection in vorticity field

Convection calculation in vorticity field is similar to solution to non-viscosity Euler equation. When the vorticity field is discrete as Eq. (7), the velocity of vortex element can be calculated by Biot-Savart integrating. Based on the Lagrange theory, convection calculation can be equivalent to solving the following ODE equation set.

$$\frac{d\boldsymbol{x}_i(t)}{dt} = \boldsymbol{u}_i(\boldsymbol{x}, t) = \boldsymbol{U}_\infty(t) + \boldsymbol{u}_f(\boldsymbol{x}_i, t) + u_0(\boldsymbol{x}_i, t) \doteq \boldsymbol{U}_\infty(\boldsymbol{x}_i, t) + u_\sigma(\boldsymbol{x}_i, t) + u_0(\boldsymbol{x}_i, t) \tag{14}$$

in which, $\boldsymbol{u}_f(\boldsymbol{x}_i, t) = -\frac{1}{2\pi}\iint_f \frac{\omega' \times (x' - x_i)}{|x' - x_i|^2} df'$, $u_\sigma(\boldsymbol{x}_i, t) = -\frac{1}{2\pi}\sum_{\substack{j=1 \\ j \neq i}}^{N} \Gamma_j K_\sigma(x_i - x_j)$; $u_0(\boldsymbol{x}, t)$ includes the influence of movement of bluff body. $K_\sigma(\boldsymbol{r})$ is the kernel function of smooth velocity.

When Eq. (14) is directly solved, the computing times for one step has the magnitude of $O(N^2)$. Here, N is the number of vortex element. In this paper, fast multipole method (Carrier *et al*. 1988) is applied for convection calculation of vortex elements.

3.2 Vorticity diffusion calculation simulated by particle strength exchange method

The most fundamental rule for particle strength exchange method is replacing Laplace operator by integral operator. If it is assumed that smooth function ζ meets a certain moment characteristics, and let $\Gamma_i = \omega_i S_i$, convection function $\frac{\partial \omega}{\partial t} = \nu \nabla^2 \omega$ can be written as

$$\Gamma_i^n = \Gamma_i^{n-1} + \frac{2\nu}{\sigma^2}\sum_{j=1}^{N} \zeta_\sigma(x_i - x_j)(\Gamma_j^{n-1} S_i - \Gamma_i^{n-1} S_j) \tag{15}$$

In actual practice, because of rapid decreasing of ζ, only particles near particle i will have obvious influence on $d\Gamma_i/dt$. In order to reduce computing amount, only particles near particle i are considered. The particle sets which have obvious influence on $d\Gamma_i/dt$ are named as D_i. If Gaussian smoothing is applied, D_i includes all particles with the distance of $\bar{x}_i$ less than 5σ.

$$\Gamma_i^n \cong \Gamma_i^{n-1} + \frac{2\nu}{\sigma^2}\sum_{j \in D_i} \zeta_\sigma(x_i - x_j)(\Gamma_j^{n-1} S_i - \Gamma_i^{n-1} S_j) \tag{16}$$

4. Redistribution of particle strength

In order to simulate the diffusion correctly, every particle should be surrounded by other particles, which can make easy exchange of their circulation by particle strength method. Except the initial inhomogeneous distribution of particles, the internal features of Lagrange method are losing overlapping and generating too many overlapping in flow with the growth of time. The main reason for this phenomenon is that the deformation of flow makes particles in flow to gather in one direction, and diffuse in the other direction, which leads to inhomogeneous distribution of particles.

In particle strength method, redistribution is an absolutely necessary step.

In this paper, old particles are covered by newly mesh. What to do next is how to interpolate locations of old vortex regions and deformed particles to new particles and new vortex regions.

$$\tilde{\omega}(\tilde{x}) \approx \omega(x) \tag{17}$$

If $\tilde{\Gamma}$ and Γ represent new and old particle strengths, correct interpolating kernel can be determined as

$$\tilde{\Gamma}_i(\tilde{x}_i) \approx \sum^{M} \Gamma_j(x_j)\Lambda(\tilde{x}_i - x_j) \tag{18}$$

Fourier transformation can be used to determine interpolating kernel. In this paper, interpolating kernel Λ_3 is applied, which keep the conservation of first moment, second moment and third moment of vorticity. For the case of one dimension, Λ_3 can be shown as Fig. 3.

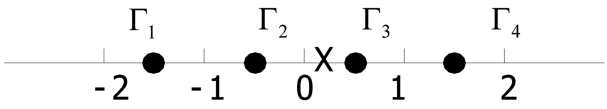

Fig. 3 Redistribution of new and old particles in Λ_3

$$\begin{cases} \Gamma_1 + \Gamma_2 + \Gamma_3 + \Gamma_4 = 1 \\ \Gamma_1 \times \left(-\frac{3}{2}\right) + \Gamma_2 \times \left(-\frac{1}{2}\right) + \Gamma_3 \times \frac{1}{2} + \Gamma_4 \times \frac{3}{2} = x \\ \Gamma_1 \times \frac{9}{4} + \Gamma_2 \times \frac{1}{4} + \Gamma_3 \times \frac{1}{4} + \Gamma_4 \times \frac{9}{4} = x^2 \\ \Gamma_1 \times \left(-\frac{27}{8}\right) + \Gamma_2 \times \left(-\frac{1}{8}\right) + \Gamma_3 \times \frac{1}{8} + \Gamma_4 \times \frac{27}{8} = x \end{cases} \Rightarrow \begin{cases} \Gamma_1 = (3-2x)(4x^2-1)/48 \\ \Gamma_2 = (1-2x)(9-4x^2)/16 \\ \Gamma_3 = (1+2x)(9-4x^2)/16 \\ \Gamma_4 = (3+2x)(4x^2-1)/48 \end{cases} \tag{19}$$

5. Calculation of aerodynamic forces

When applying equation of moment of momentum at the boundary of bluff body, the form for fixed coordinate is

$$\boldsymbol{s} \cdot \left.\frac{d\boldsymbol{u}}{dt}\right|_S = -\left.\frac{1}{\rho}\frac{\partial p}{\partial \boldsymbol{s}}\right|_S + \nu \left.\frac{\partial \omega}{\partial \boldsymbol{n}}\right|_S \tag{20}$$

According to assumption of simplification of boundary layer, the diffusion effect of vorticity in the tangent direction of boundary can be neglected. Considering $\frac{\partial \gamma}{\partial n} = \omega$ and $\frac{\partial \gamma}{\partial t} = \nu \frac{\partial \omega}{\partial \boldsymbol{n}}$, in the meaning of discretization, Eq. (20) can be rewritten as

$$\left(\frac{\partial p}{\partial s}\right)_i^n = -\frac{\gamma_i(n\Delta t) - \gamma_i^a(n\Delta t)}{\Delta t} - a_{si}^n \tag{21}$$

In which, $\gamma_i(n\Delta t)$ is the strength of vortex sheet generated at the time of $n\Delta t$, $\gamma_i^q(n\Delta t)$ is equivalent strength of the vortex sheet entering bluff body from time $(n-1)\Delta t$ to $n\Delta t$, a_{si}^n is the acceleration in the tangent direction of i-th control point at the time of $n\Delta t$.

According to the discretization form of Eq. (21), the drag force, lift force and pitching moment can be obtained by integrating the distribution of pressure along the surface of boundary.

6. Reynolds number effect analysis

6.1 Parameters for PSE calculations

The parameters in different Reynolds number are listed in Table 1, and the reference dimension for aerostatic force coefficients is the height of deck sections.

6.2 Reynolds number effect on force coefficients and Strouhal number

6.2.1 Great Belt East Bridge

Table 2 gives comparisons of drag coefficients and Strouhal number by PSE in this paper with RVM (Zhou *et al*. 2003, Zhou and Chen 2006), RVM (Schewe and Larsen 1998), 2D FEM method (Selvam 2000), 3D FEM method and experimental results. The curves of drag coefficient lift force coefficient and pitching moment coefficient of Great Belt East Bridge varying with Reynolds number is shown in Fig. 4. Fig. 5 gives contour plot of vorticity in flow. Fig. 6 gives the comparison of contour plot of vorticity in flow between PSE and RVM.

Table 1 Parameters for PSE calculation of Great Belt East Bridge and Sutong Bridge

	R_e	Number of SVS*	Time step	Grid spacing	Integration scheme for convection	Integration scheme for diffusion	Integration scheme for convection of surface vorticity
Great Belt East Bridge	1E4	154	0.005	0.008	Euler	Euler	3 points Gaussian
	1E5	445	0.005	0.006	Euler	Euler	3 points Gaussian
	2E5	445	0.005	0.006	Euler	Euler	3 points Gaussian
	5E5	445	0.005	0.006	Euler	Euler	3 points Gaussian
	1E6	445	0.005	0.005	Euler	Euler	3 points Gaussian
Sutong Bridge	2E5	208	0.007	0.01	Euler	Euler	4 points Gaussian
	5E5	208	0.007	0.01	Euler	Euler	4 points Gaussian
	6E5	208	0.007	0.01	Euler	Euler	4 points Gaussian
	8E5	208	0.006	0.01	Euler	Euler	4 points Gaussian
	1E6	208	0.005	0.005	Euler	Euler	4 points Gaussian
	1.1E6	208	0.005	0.005	Euler	Euler	4 points Gaussian
	1.2E6	208	0.005	0.005	Euler	Euler	4 points Gaussian
	1.4E6	208	0.005	0.005	Euler	Euler	4 points Gaussian

*SVS, surface vortex sheet

Table 2 Comparison of drag force coefficients and Strouhal number

methods	PSE	RVM	RVM (Walther)	2DFEM (Selvam)	3DFEM (Selvam)	Experimental results (Walther)
C_d	0.1994	0.1936	0.179	0.35	0.236	0.19
St	0.152	0.167	0.190	0.236	0.17	0.17

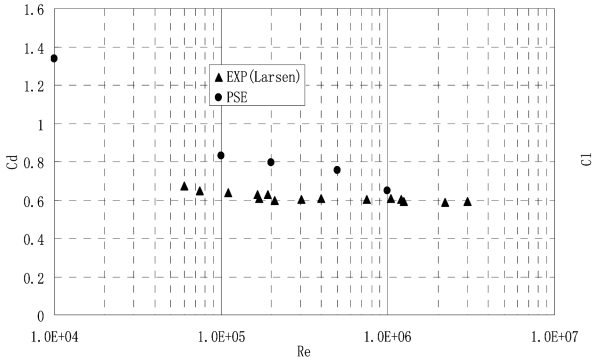

(a) Drag force coefficients

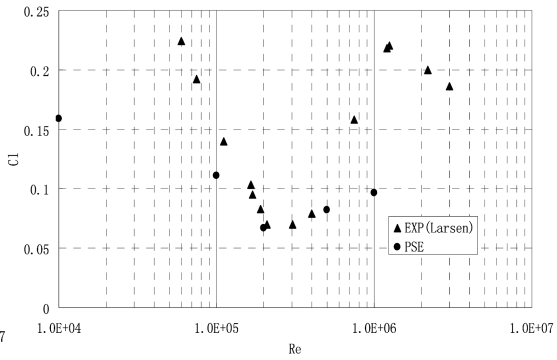

(b) Lift force coefficients

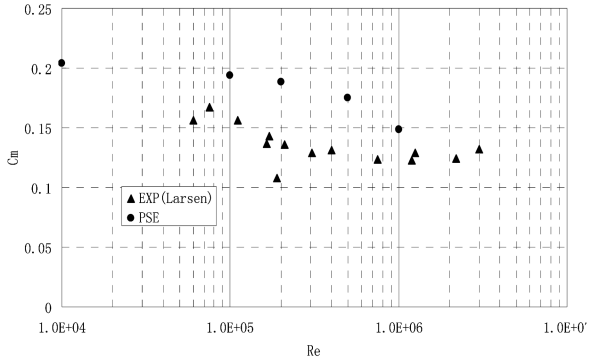

(c) Pitching moment coefficient

Fig. 4 Aerostatic coefficients at attack angle of 0 deg vs. Reynolds number (Great Belt East Bridge)

Fig. 5 Contour plot of vorticity in flow by PSE (Great Belt East Bridge)

From the comparison of drag force coefficient with those obtained by Schewe and Larsen (1998), it can be seen that the tendency of the results obtained by PSE approximate well to the experimental results. Both drag coefficients decreases with R_e. But the results by PSE are slightly higher than the experimental results. From Fig. 4(a), it can be found that the results by PSE are approximate well to experimental results with the R_e ranging from 2×10^5 to 5×10^5. But the results by PSE are slightly

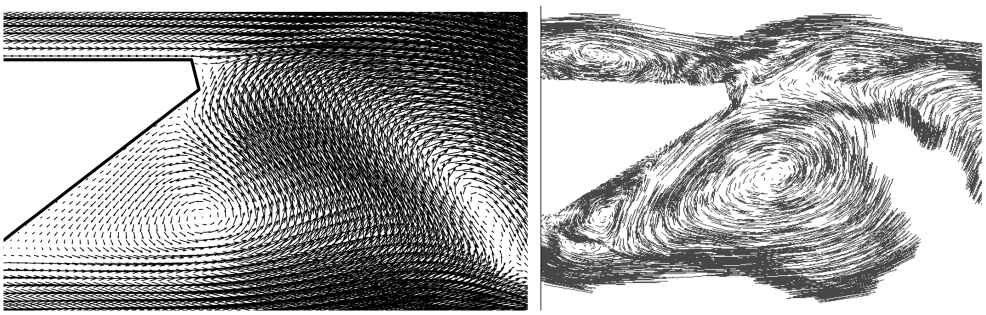

Fig. 6 Contour plot of vorticity in flow by PSE and RVM (Great Belt East Bridge)

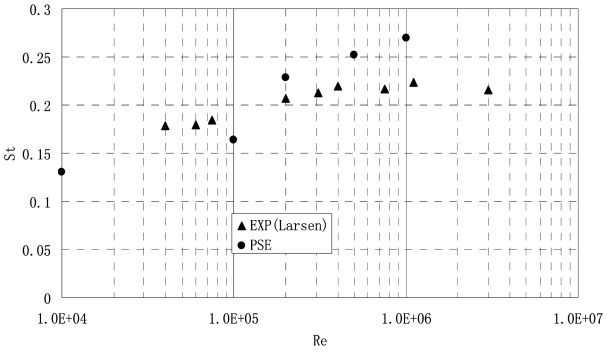

Fig. 7 Strouhal number at attack angle of 0^o vs. the Reynolds number (Great Belt East Bridge)

smaller than experimental results with the R_e ranging from 1×10^4 to 1×10^6. Small absolute value, large volatility and unstable data of lift coefficient may be the reasons for the inconsistency. The influence of the Reynolds number on lift coefficients is more complicated than that on drag force coefficient.

Strouhal number is a non-dimensional number related to vortex shedding phenomena. The Strouhal number is directly correlated to vortex induced vibration (VIV) lock-in wind speed. Therefore, investigation of the Reynolds number effect on Strouhal number has significant meaning to VIV lock-in wind speed. Strouhal number can be obtained by FFT transformation of time history of aerostatic forces. For the deck of Great Belt East Bridge, the Strouhal number are given in Fig. 7 and compared with experimental results. It can be seen that the results obtained by PSE fit well with experimental results. The Strouhal number of the section increases with Reynolds number. It can be concluded that the Strouhal number is highly affected by the Reynolds number.

6.2.2 Sutong Bridge

Fig. 8 gives the curves of drag coefficient, lift coefficient and pitching moment coefficient of Sutong Bridge varying with the Reynolds number. Fig. 9 shows the contour plot of vorticity in flow. Fig. 10 shows instant flow pattern around the deck section. As shown in Fig. 8, drag force coefficient of Sutong Bridge by PSE fit well with experimental results. Both of them decrease with

Reynolds number, which is the same as the conclusion for Great Belt East Bridge. Meanwhile, both the calculated results and experimental results show that lift coefficients increase with the Reynolds number firstly, and decrease after its maximum value is arrived. Also it can be found that the pitching moment coefficient varies with the Reynolds number significantly.

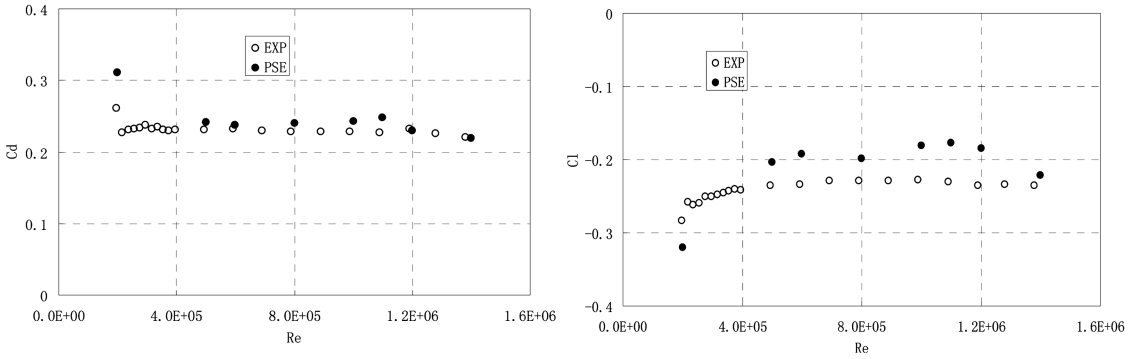

(a) Drag force coefficients (b) Lift force coefficients

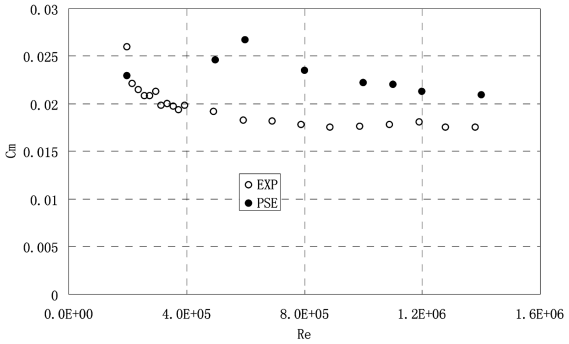

(c) Pitching moment coefficient

Fig. 8 Contour plot of vorticity in flow by PSE and RVM (Sutong Bridge)

Fig. 9 Contour plot of vorticity in flow by PSE (Sutong Bridge)

Fig. 10 Instant flow patterns around the deck section (Sutong Bridge)

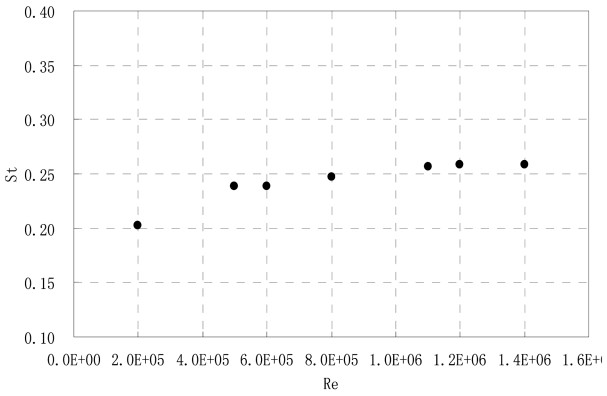

Fig. 11 Strouhal number at attack angle of 0° vs. Reynolds number (Sutong Bridge)

For the deck of Sutong Bridge, the Strouhal number is give in Fig. 11. The same conclusion can be made that the Strouhal number is also affected by the Reynolds number.

6.3 Reynolds number effect on pressure distribution

The pressure distribution of the deck cross section of Sutong Bridge at the attack angle of 0 degree is shown in Fig. 12. It can be found that the distribution of experimental values and the calculated values of surface pressure is nearly the same. So we can make the conclusion that the PSE can reproduce the wind tunnel test.

Figs. 13 and 14 shows the distribution of pressure coefficient of the lower surface and upper surface under different Reynolds numbers individually. For the lower surface, the pressure coefficient gradually decreases to the minimum with the distance to the front edge increasing, where it is called the first accelerated range. The position of the minimum remains almost unchanged, but the minimum value varies with the Reynolds number. As the distance increase, the pressure coefficient enters into the inverse-pressure gradient range, where the pressure increases and it is called the first inverse-pressure gradient range. When the pressure coefficient reaches a certain value, the pressure begins to decrease and the flow accelerates again. This section is called the second accelerated range. But both the intensity and scope of this section are much smaller compared to the first accelerated range. After the pressure coefficient passes the second minimum value, the pressure coefficient will rise again until the end of the lower surface, where it is defined as the second inverse-pressure gradient range.

The pressure coefficient distribution of lower surface and upper surface of the Great Belt East Bridge is much similar to the one of Sutong Bridge, seen in Figs. 15 and 16. The pressure coefficient distribution of lower surface of the Great Belt East Bridge can be divided into four

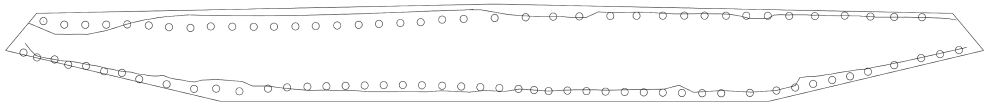

Fig. 12 The distribution of mean pressure coefficient (Sutong Bridge) ($R_e = 4 \times 10^5$, attack angle 0°, the experimental values: solid line; the calculated values: circular points; both negative for the internal section)

ranges as that of Sutong Bridge. But the pressure coefficient distribution of upper surface can be divided into three ranges, which is different from Sutong Bridge. However, it is obvious to find that the pressure distribution is highly affected by the Reynolds number, which leads to high dependency of aerostatic coefficients and Strouhal number on the Reynolds number.

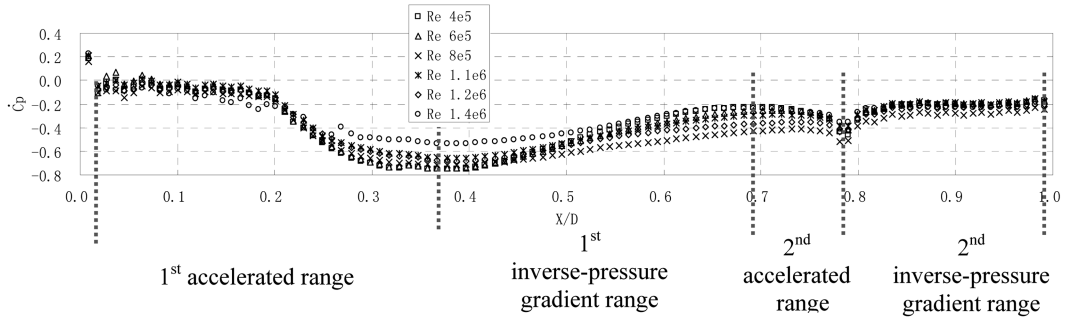

Fig. 13 The pressure distribution of lower surface of Sutong Bridge (the attack angle of 0°)

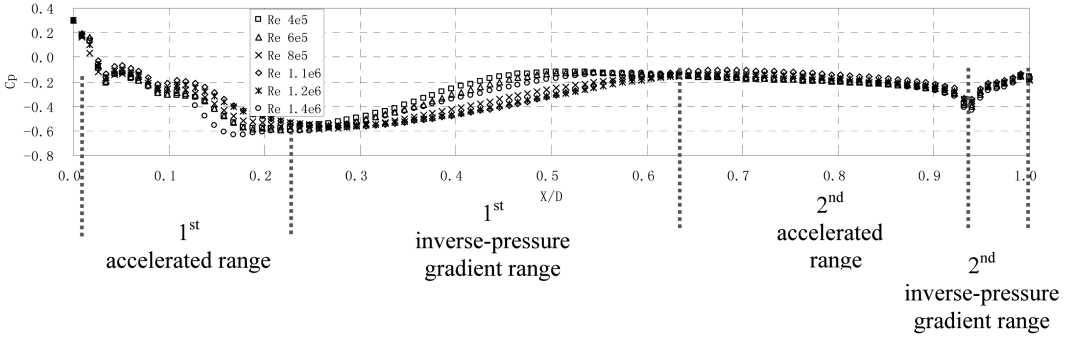

Fig. 14 The pressure distribution of upper surface of Sutong Bridge (the attack angle of 0°)

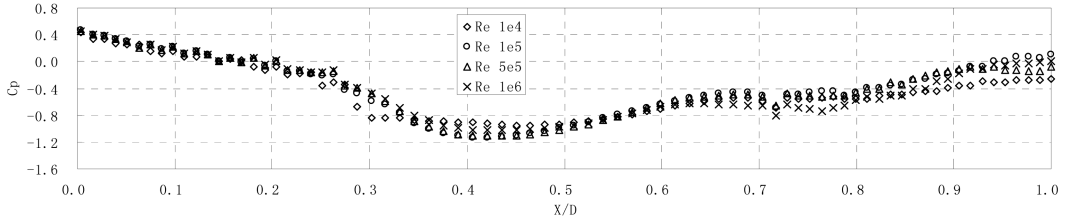

Fig. 15 The pressure distribution of lower surface of the Great Belt East Bridge (the attack angle of 0°)

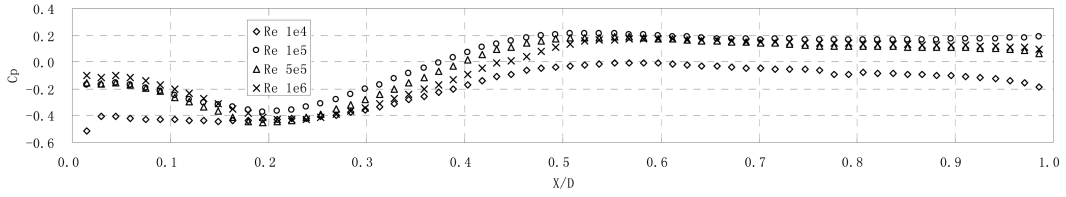

Fig. 16 The pressure distribution of upper surface of the Great Belt East Bridge (the attack angle of 0°)

7. Conclusions

In this paper, aerostatic force coefficients and Strouhal numbers of Sutong Bridge and the Great Belt East Bridge at attack angle of 0° by PSE are investigated. Compared with experimental results as well as results from some other literatures, it can be found that PSE is able to reproduce the Reynolds number effect. From the varying rules of aerostatic force coefficients and the Strouhal number of two deck sections vs. the Reynolds number, it can also be concluded that the Reynolds number effect on aerostatic force coefficients and the Strouhal number should not be neglected. Especially when Reynolds number is in the range from 10^5 to 10^6, the Strouhal numbers are strongly influenced by Reynolds number. It can also be concluded that the pressure distribution is highly affected by the Reynolds number, which leads to high dependency of aerostatic coefficients and Strouhal number on the Reynolds number.

Acknowledgements

The project is jointly supported by National Science Foundation under Grant No. 50878148, Grant No. 50708073, and National Key Technologies R&D Program under Grant No. 2006BAG04B01, which are gratefully acknowledged.

References

Barré, C. and Barnaud, G. (1995), "High Reynolds number simulation techniques and their application to shaped structures model test", *J. Wind Eng. Ind. Aerod.*, **57**(2-3), 145-157.

Carrier, J., Greengard, L. and Rokhlin, V. (1988), "A fast adaptive multipole algorithm for particle simulations", *SIAM J. Sci. Comput.*, **9**(4), 669-686.

Chen, A.R. (2004), *Experimental Study on vortex excited vibration and aerodynamic force coefficients of the girder of Sutong Bridge under high Reynolds number (Report in Chinese)*, Shanghai, SKLDRC, Tongji University.

Chen, A.R., Zhou, Z.Y. and Xiang, H.F. (2006), "On the mechanism of vertical stabilizer plates for improving aerodynamic stability of bridges", *Wind Struct.*, **9**(1), 59-74.

Choquin, J.P. and Huberson, S. (1989), "Particles simulation of viscous flow", *Comput. Fluids*, **17**(2), 397-410.

Choquin, J.P. and Lucquin-Desreux, B. (1988), "Accuracy of a deterministic particle method for Navier-Stokes equations", *Int. J. Numer. Meth. Fl.*, **8**(11), 1439-1458.

Chorin, A.J. (1973), "Numerical study of slightly viscous flow", *J. Fluid Mech.*, **57**(4), 785-796.

Cottet, G.H. (1990), "A particle-grid superposition method for the Navier-Stokes equations", *J. Comput. Phys.*, **89**(2), 301-318.

Degond, P. and Mas-Gallic, S. (1989), "The weighted particle method for convection-diffusion equations. Part 1: The case of an isotropic viscosity", *Math. Comput.*, **53**(188), 485-507.

Eldredge, J.D., Leonard, A. and Colonius T. (2002), "A general deterministic treatment of derivatives in particle methods", *J. Comput. Phys.*, **180**(2), 686–709.

Fishelov, D. (1990), "A new vortex scheme for viscous flows", *J. Comput. Phys.*, **86**(1), 211-224.

Koumoutsakos, P., Leonard, A. and Pépin, F. (1994), "Boundary conditions for viscous vortex methods", *J. Comput. Phys.*, **113**(1), 52-61.

Leonard, A. (1980), "Vortex methods for flow simulation", *J. Comput. Phys.*, **37**(3), 289-335.

Ploumhans, P. and Winckelmans, G.S. (2000), "Vortex methods for high-resolution simulations of viscous flow past bluff bodies of general geometry", *J. Comput. Phys.*, **165**(2), 354-406.

Sarpkaya, T. (1989), "Computational methods with vortices - the 1988 freeman scholar lecture", *J. Fluid. Eng.-T. ASME*, **111**, 5-52.
Scanlan, R. (1975), "Theory of the wind analysis of long-span bridges based on data obtainable from section model tests", *Proceedings of the 4th international Conference on wind effects on Buildings and Structures*, London.
Schewe, G. (2001), "Reynolds number effects in flow around more-or-less bluff bodies", *J. Wind Eng. Ind. Aerod.*, **89**(14-15), 1267-1289.
Schewe, G. (1983), "On the force fluctuations acting on a circular cylinder in cross flow from subcritical up to transcritical Reynolds numbers", *J. fluid Mech.*, **133**, 265-285.
Schewe, G. and Larsen, A. (1998), "Reynolds number effects in the flow around a bluff bridge cross section", *J. Wind Eng. Ind. Aerod.*, **74-76**(1), 829-838.
Selvam, R.P. (2000), *Computational procedures in grid based computational bridge aerodynamics* (Eds. Larsen, A., Esdahl, S.), Bridge Aerodynamics, A.A. Balkema, Rotterdam.
Shankar, S. and Van Dommelen, L. (1996), "A new diffusion procedure for vortex methods", *J. Comput. Phys.*, **127**(1), 88-109.
Taylor, I. and Vezza, M. (1999), "Calculation of the flow field around a square section cylinder undergoing forced transverse oscillations using a discrete vortex method", *J. Wind Eng. Ind. Aerod.*, **82**(1-3), 271-291.
Walther, J.H. and Larsen, A. (1997), "Two dimensional discrete vortex method for application to bluff body aerodynamics", *J. Wind Eng. Ind. Aerod.*, **67-68**, 183-193.
Winckelmans, G.S. and Leonard, A. (1993), "Contributions to vortex particle methods for the computation of three dimensional incompressible unsteady flows", *J. Comput. Phys.*, **109**(2), 247-273.
Zhou, Z.Y., Chen, A.R. and Xiang, H.F. (2003), "Identification of aeroelastic parameter of flexible bridge decks by random discrete vortex method", *Proceedings 11th International Conference on Wind Engineering*, Lubbock, Texas, USA, June.
Zhou, Z.Y. and Chen, A.R. (2006a), "On the mechanism of torsional flutter instability for 1st Tacoma Narrow Bridge by discrete vortex method", *Proceedings of the fourth International Symposium on Computational Wind Engineering*, Yokohama, Japan, July.
Zhou, Z.Y. and Chen, A.R. (2006b), "Effect of additional attack angle on flutter stability", *Proceedings of the 12th International Conference on Wind Engineering*, Cairns, Australia, July.

CC